Nanoporous Fe-based alloy prepared by selective dissolution: an effective Fenton catalyst for water remediation

Huiyan Zhang[a], Yuping Feng[a], Yangyang Cheng[b], Maria Dolors Baró[a], Ainhoa Altube[c], Eva García-Lecina[c], Francisco Alcaide[d], Eva Pellicer[a,], Tao Zhang[b], Jordi Sort[a,e,§]*

[a] Departament de Física, Building Cc, Universitat Autònoma de Barcelona, Cerdanyola del Vallès, Barcelona, E08193, Spain.

[b] Key Laboratory of Aerospace Materials and Performance (Ministry of Education), School of Materials Science and Engineering, Beihang University, 37 Xueyuanlu, Haidian District, Beijing, 100191, China.

[c] Unidad de Superficies Metálicas, IK4-CIDETEC, Paseo Miramón 196, Donostia-San Sebastián, Gipuzkoa, E20009, Spain.

[d] Unidad de Nuevas Tecnologías para la Energía, IK4-CIDETEC, Paseo Miramón 196, Donostia-San Sebastián, Gipuzkoa, E20009, Spain.

[e] Institució Catalana de Recerca i Estudis Avançats (ICREA), Passeig Lluís Companys 23, E08010 Barcelona, Spain.

To whom correspondence should be addressed: *eva.pellicer@uab.cat; §jordi.sort@uab.cat

Additional authors' information (e-mail addresses of all authors): Huiyan Zhang (abuzhang1984@gmail.com); Yuping Feng (fengyupingcsu@gmail.com); Yangyang Cheng (chengyangyang@buaa.edu.cn); Maria Dolors Baró (dolors.baro@uab.cat); Ainhoa Altube (Aaltube@cidetec.es), Eva García-Lecina (egarcia@cidetec.es); Francisco Alcaide (falcaide@cidetec.es); Eva Pellicer (eva.pellicer@uab.cat); Tao Zhang (zhangtao@buaa.edu.cn); Jordi Sort (jordi.sort@uab.cat)

Abstract:

Fully nanoporous Fe-rich alloy, prepared by selective dissolution of melt-spun $Fe_{43.5}Cu_{56.5}$ ribbons, exhibits outstanding properties as heterogeneous Fenton catalyst towards the degradation of methyl orange (MO) in aqueous solution. In addition, the ferromagnetic characteristics of this material enable its wireless manipulation towards specific locations within polluted wastewater. The influence of selective dissolution on the microstructure, sample morphology (surface and cross section), elemental composition and magnetic properties of the resulting nanoporous alloy are investigated. The dealloying procedure enhances the saturation magnetization and drastically increases the catalytic performance (i.e., the time required for full degradation of MO from the media is reduced by approximately a factor of 2 by subjecting the $Fe_{43.5}Cu_{56.5}$ ribbons to prior dealloying). Remarkably, the effectiveness of this nanoporous material surpasses the results obtained by homogeneous Fenton reaction using the equivalent concentration of Fe cations leached into the media from the nanoporous alloy. The different factors that promote the high catalytic activity are discussed. The outstanding catalytic activity, together with the simplicity of the synthetic procedure, makes this material very appealing for water remediation using advanced Fenton processes.

Keywords: nanoporous structure, Fe-based alloy, electrochemical dealloying, Fenton reaction, water remediation

1. Introduction

With the massive growth of industrial and agricultural activities, water pollution has become one of the major environmental threats to human health and ecosystems in general.[1] During the last decades, various types of physical, chemical and biological methods have been put forward to remove non-degradable organic compounds from industrial wastewater. However, most of these methods suffer from important drawbacks. For instance, physical methods such as liquid-liquid extraction or ion-exchange are ineffective for pollutants that are not easily adsorbable or volatile. Membrane filtration requires very high water pressure, which in turn causes large energy power consumption. Activated carbon adsorption processes are also very costly.[2] Ozone and hypochlorite oxidation processes are efficient, but the costly equipment and the secondary pollution produced by the residual chlorine make them undesirable.[3] In fact, many of these methods simply convert the pollutants to other compounds, rather than actually eliminating them.[4]

Remarkably, some advanced chemical oxidation processes can induce almost complete mineralization of a widespread range of organic pollutants. For example, Fenton reactions (i.e., iron catalyzed hydrogen peroxide) can either oxidize the contaminant materials to smaller organic molecules or transform them into water, carbon dioxide and salts.[5-13] Besides water remediation, Fenton reaction is also of interest in biological applications since it involves the

creation of free radicals by chemicals that are present in bodily fluids. Some additional advantages of the Fenton reaction are its high efficiency, simplicity in destroying the contaminants, or the non-necessity of sophisticated equipment.[14] Moreover, the reaction takes place in ambient conditions.[15] For these reasons, homogeneous Fenton catalysts (in which Fe cations are directly dissolved in the liquid media) have been widely investigated and are now considered as a promising strategy for wastewater treatment.[16]

As an alternative to homogeneous Fenton, some attempts have been made to develop "heterogeneous" Fenton catalysts, i.e., solid materials that are immersed, but not dissolved, in the media while providing a high catalytic activity. In principle, some of the limitations encountered by homogeneous process might be overcome by heterogeneous Fenton oxidation processes.[17,18] Namely, it has been reported that heterogeneous Fenton oxidation exhibits lower activation free energy than homogeneous Fenton reaction.[19] Furthermore, during heterogeneous Fenton reaction, high amounts of surface active sites for H_2O_2 decomposition and formation of hydroxyl radicals are available, sometimes inducing a higher removal efficiency compared to homogeneous Fenton process.[20] Heterogeneous Fenton catalysts can be prepared by incorporating Fe ions, zero-valence iron (ZVI) or Fe oxide phases (e.g., in the form on nanoparticles) inside porous scaffolds that act as support materials (e.g., zeolites, nafion, clay or activated carbon).[21-23] Nevertheless, since the host material is inactive toward the Fenton reaction, the benefit brought by the large porosity is not exploited to the full. In other words, the amount of available surface area exposed to the solution (i.e., active sites where the reactant molecules can be adsorbed) is limited to the nanoparticles. For this reason, a fully porous active material, instead of active particles embedded in a porous support, might be a suitable alternative

to enhance the Fenton efficiency. In any case, mechanical integrity of the nanoporous materials is a critical issue, in order to use them for heterogeneous catalysis experiments.

Interestingly, it has been shown that mixed iron/copper species may also promote Fenton-like processes while allowing for a less critical dependence on the pH value. Indeed, bimetallic Fe-Cu nanoparticles introduced inside different types of two-dimensional or three dimensional porous frameworks have shown large potential for heterogeneous Fenton catalytic activity.[24-26] Furthermore, since Fe-based materials are often ferromagnetic, this allows precise guiding of the catalysts towards specific locations of the polluted water by means of externally applied magnetic field and field gradients, while also offering the possibility to recover them after usage for recycling purposes.[27]

During the last few years, progress has been made towards the development of nanoporous metallic materials by means of dealloying (i.e., selective removal of the less noble element from an alloy, by either chemical or electrochemical means).[28] The process can be applied to various combinations of binary or ternary alloys, such as Ag-Au, Pt-Al, Al-Pd-Au, Ni-Mn, Ni-Pd or Fe-Cu, among others. In particular, it has been reported that the phase separated Fe-Cu binary alloy with composition around $Fe_{43}Cu_{57}$ can be selectively etched to remove Cu and render Fe-rich metallic alloy featuring nanometer sized pores.[29] Although detailed structural characterization of this type of material has been previously reported,[29] most of its physical and catalytic properties, as well as its potential applications, have been largely overlooked. In this study, three-dimensional nanoporous Fe-rich alloy is prepared by dealloying $Fe_{43.5}Cu_{56.5}$ ribbons previously synthesized by rapid solidification (see Figure 1). The phase structure, morphology, elemental composition and magnetic properties of the ribbons before and after selective dissolution are investigated in detail. The degradation performance of methyl orange (MO) during Fenton

reaction when using dense as-spun and nanoporous dealloyed ribbons is assessed. Remarkably, the nanoporous material outperforms the as-quenched non-dealloyed sample. The highly efficient catalytic activity and the convenient processing method make this nanoporous catalyst a prospective new candidate for heterogeneous Fenton chemistry.

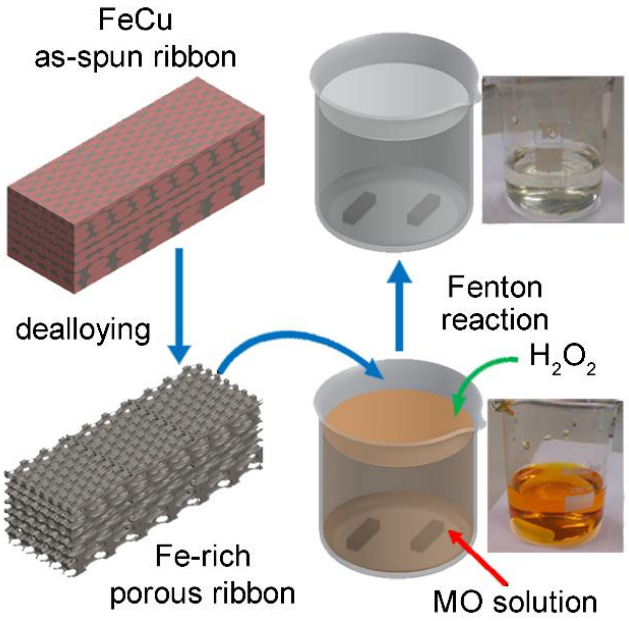

Figure 1. Schematic drawing of the dealloying process used to obtain Fe-rich nanoporous ribbons and the efficiency of the as-spun FeCu and dealloyed ribbons for degradation of methyl-orange using Fenton reaction.

2. Results and Discussion

2.1 Structural and Morphological Characterization

As shown in the X-ray diffraction (XRD) patterns of Figure 2, the typical peaks of *fcc*-Cu and *bcc*-Fe phases can be identified in the as-spun ribbon, which indicates the occurrence of phase

separation. However, after selective etching, the peaks from *fcc*-Cu almost vanished while those from *bcc*-Fe remain clearly visible. This demonstrates that the dealloying treatment is very effective in drastically reducing the amount of *fcc*-Cu phase.

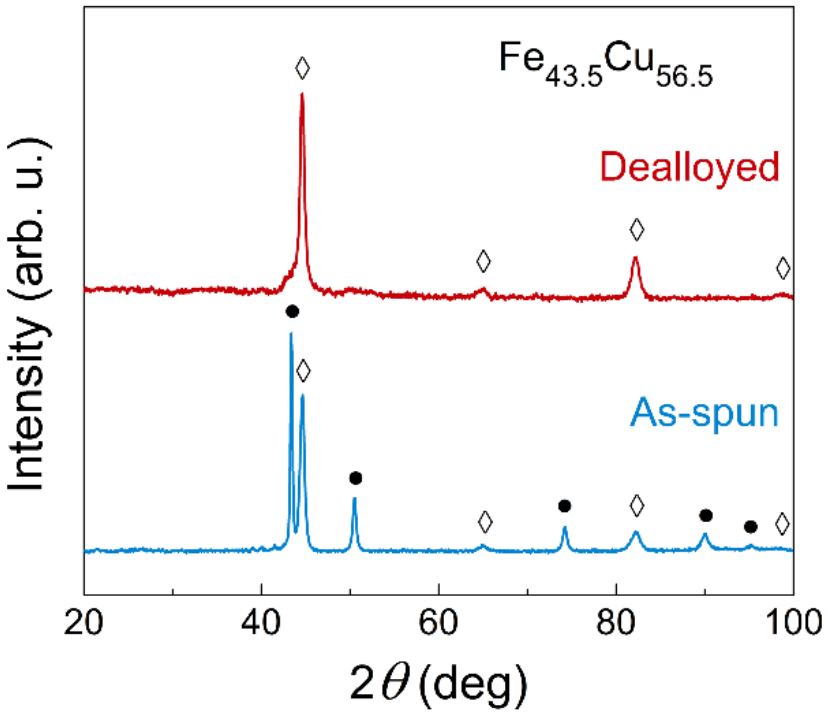

Figure 2. XRD patterns of $Fe_{43.5}Cu_{56.5}$ alloy before and after selective dissolution in 0.1M HNO_3 at an applied voltage of 14 V for 5 min. The peaks correspond to *fcc*-Cu (•) and *bcc*-Fe (◊) phases separately.

The gradient of cooling rate across the ribbon during melt-spinning causes a variation of the surface morphology and microstructure between the free-side and the wheel-side of the as-spun ribbon.[30] Field-emission scanning electron microscopy (FESEM) images of both sides of the ribbon, as well as its cross section, for the as-spun and dealloyed states, are displayed in Figure 3. Compared with the rather dense appearance of the as-spun ribbon (Figure 3a), a fully porous

morphology is observed after selective etching (Figure 3b). However, the pore size of the dealloyed sample varies from ~50-100 nm to ~500 nm when comparing the wheel-side with the free-side (cf. Figure 3b and c). To some extent, this could actually be anticipated, since the microstructure at the wheel side (faster cooling rate) is more refined than that at the air-side. The ligaments are rather elongated and mostly oriented parallel to the ribbon plane, their size varying between ~50 nm and ~300 nm.

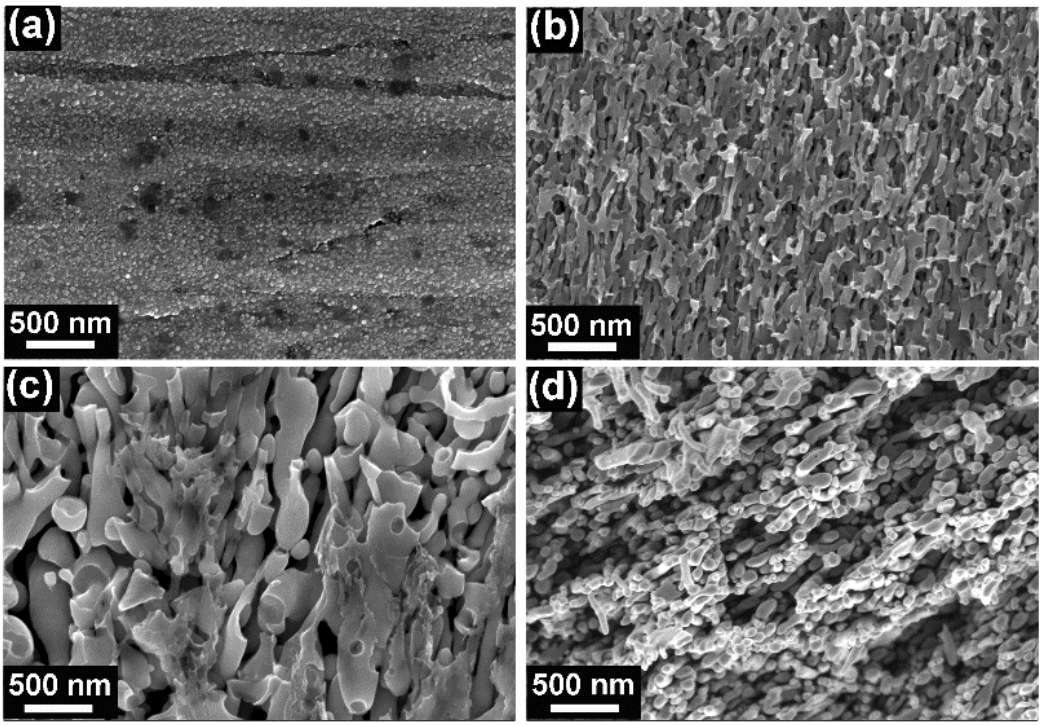

Figure 3. SEM images of (a) polished as-spun $Fe_{43.5}Cu_{56.5}$ ribbon (taken on the wheel side) and (b-d) dealloyed ribbon: (b) wheel-side, (c) free-side and (d) fracture cross section.

Cross-section analyses of the dealloyed ribbon indicated that etching and hence, the occurrence of porosity, was accomplished through the entire ribbon thickness (Figure 3d). A low magnification SEM image of the cross-section is shown in Figure S1 (Supplemental information). The compositions of the ribbons, measured by energy-dispersive X-ray (EDX)

analyses at different locations of the samples, before and after dealloying, are listed in Table 1. Slight variations in the amounts of Fe and Cu exist between the wheel and free sides of the as-spun ribbons. Remarkably, a clear enrichment in Fe is observed in the dealloyed nanoporous ribbons, which is in agreement with the XRD results. The oxygen content also increases a bit after dealloying, although it typically remains below 20 at%. The occurrence of O is likely attributed to the formation of Fe oxides during electrochemical polarization. However, oxide peaks could not be detected by XRD, indicating that the oxide layer is exceedingly thin in comparison to the penetration depth of the X-rays.

Material	Location	Chemical composition (at %)		
		Fe	Cu	O
Polished as-spun ribbon (before Fenton)	Free-side	44	52	4
	Wheel-side	39	58	3
Dealloyed ribbon (before Fenton)	Free-side	61	17	22
	Wheel-side	69	20	11
	Fracture cross-section	67	18	15
As-spun ribbon after Fenton reaction	Wheel-side	~2	66	31
	Fracture cross-section	~2	75	23
Dealloyed ribbon after Fenton reaction	Wheel-side	~3	73	24
	Fracture cross-section	~3	76	21

Table 1. Average EDX results (obtained by applying a voltage of 10 kV) from both sides of the ribbons and the cross-sections (as-spun and dealloyed), before and after Fenton reaction.

2.2 Magnetic Properties

Figure 4 shows the hysteresis loops of the as-spun and dealloyed ribbons, from which a soft ferromagnetic behavior is observed. The values of saturation magnetization (M_s), remanence (M_r) and coercivity (H_c) for both samples are listed in Table 2. In general, these two materials display similar magnetic properties, which stem from the bcc Fe-rich phase.[31] However, the nanoporous (dealloyed) Fe-rich alloy possesses higher M_s, M_r and H_c than the as-spun ribbon. The increase of M_r and M_s after dealloying can be ascribed to the removal of the paramagnetic Cu-rich phase by selective dissolution.[31,32] However, the saturation magnetization of the dealloyed ribbon is still lower than that of bulk Fe (where M_s = 218 emu g^{-1}),[33] due to the presence of Cu and O, in agreement with EDX analyses. For both samples, the values of H_c are higher than the typical ones for bulk Fe (of only a few Oe),[33] and are similar to the H_c measured in other types of Fe-based ribbons.[34] The slightly larger H_c after dealloying could be due to the hindrances for domain wall propagation imposed by the reduced lateral dimensions of the ligaments constituting the nanoporous ribbons.

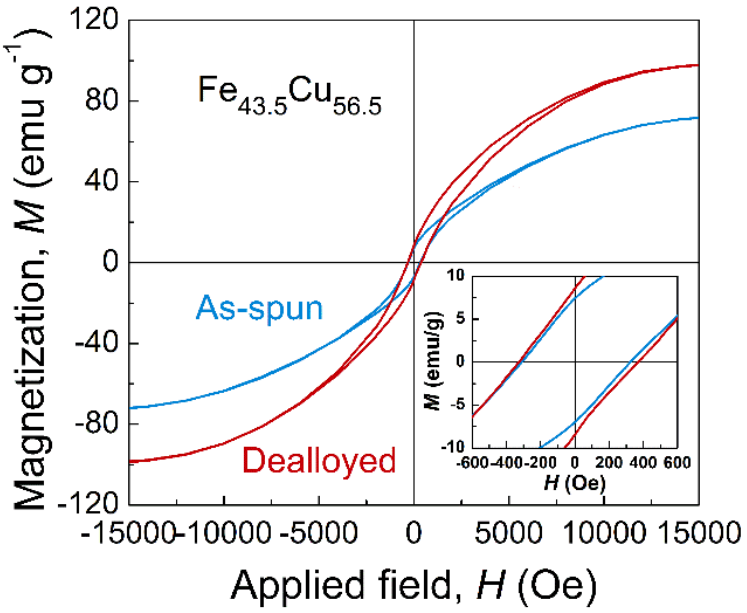

Figure 4. Hysteresis loops of $Fe_{43.5}Cu_{56.5}$ ribbons corresponding to as-spun and dealloyed states. The inset shows a magnified view at low fields.

Material	Saturation magnetization M_s, emu g^{-1}	Remanence M_r, emu g^{-1}	Coercivity H_c, Oe
Polished as-spun ribbon (before Fenton)	73.1	7.2	317.3
Dealloyed ribbon (before Fenton)	99.3	8.5	349.6
As-spun ribbon after Fenton reaction	~0.87	~0.06	197.5
Dealloyed ribbon after Fenton reaction	~0.31	~0.03	268.8

Table 2. Magnetic properties of the as-spun and dealloyed ribbons, before and after Fenton reaction.

2.3 Surface Characterization

X-ray photoemission spectroscopy (XPS) characterization of the ribbons after dealloying was carried out in order to identify eventual changes in both the oxidation state and the amounts of Fe and Cu at surface level. The survey spectra (Figure 5) showed an increase of the Fe 2p signal and, concomitantly, a decrease of the Cu 2p peak after dealloying, in agreement with EDX analyses.

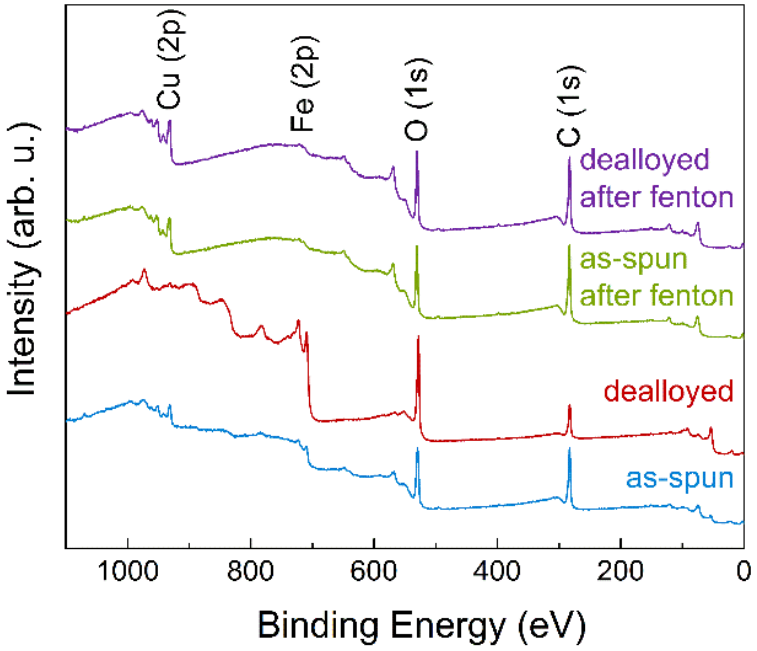

Figure 5. XPS survey spectra of the as-spun and dealloyed ribbons before and after the Fenton reaction.

The deconvoluted core-level Fe 2p spectra of the dealloyed sample are shown in Figure 6a and c. The two doublets located between 717 eV and 705 eV ($2p^{3/2}$) and between 730 eV and 720 eV ($2p^{1/2}$) indicate that iron is mostly in its oxidized state (Fe^{2+} and Fe^{3+}). Interestingly, the relative amount of Fe^{3+} in the dealloyed sample is higher than in the as-spun one (see Figure S2a for

comparison), hence indicating that the outermost surface of the dealloyed ribbon is more oxidized. The weak shoulder peak at around 706.1 eV, observed both before and after dealloying, can be ascribed to ZVI ($2p^{3/2}$). Remarkably, the ZVI signal became very strong after Ar ions sputtering (Figure 6c), by which the uttermost surface is removed.[35] Simultaneously, the contribution from oxidized Fe is strongly reduced.

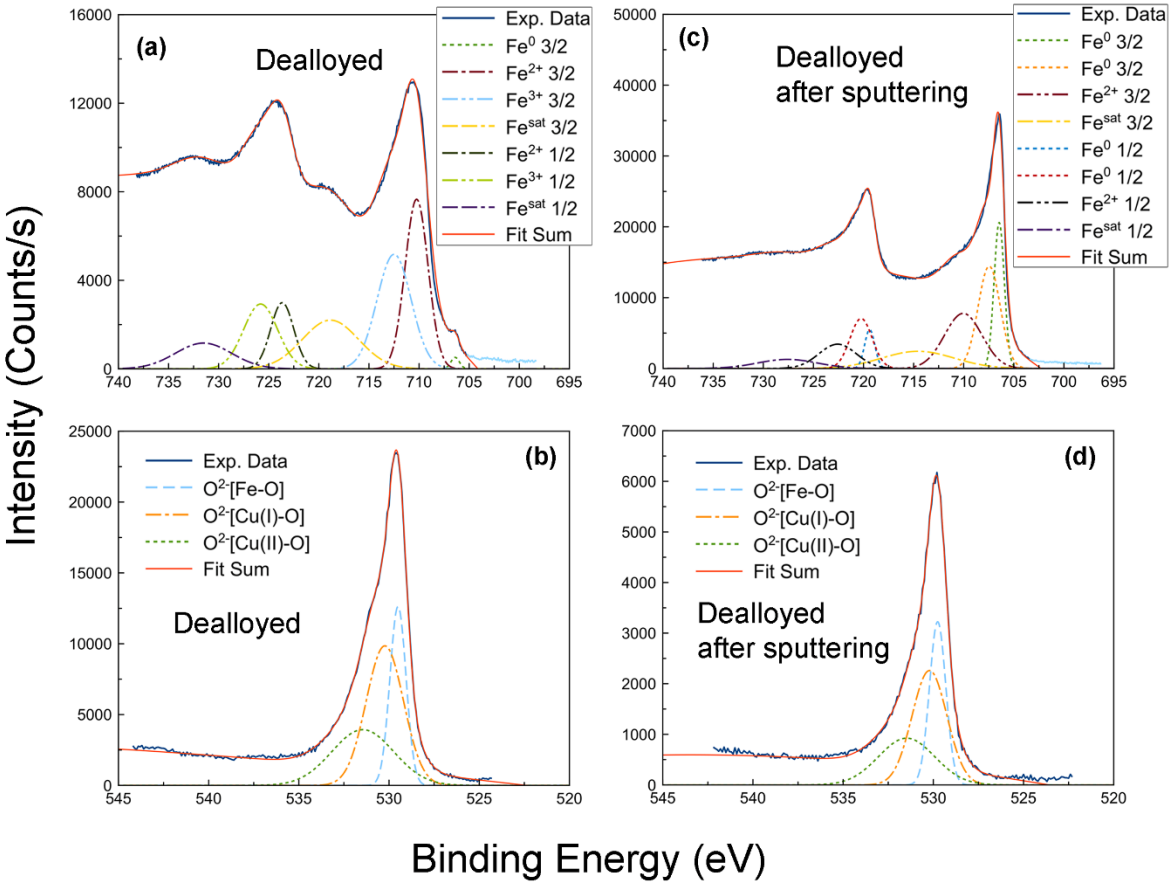

Figure 6. Experimental and deconvoluted high resolution XPS spectra of (a) Fe 2p and (b) O 1s at surface level, and of (c) Fe 2p and (d) O 1s after 1 min Ar ions sputtering for the dealloyed ribbon (before Fenton reaction).

The core-level Cu 2p spectra of the as-spun and dealloyed (the latter taken at surface level and after Ar ions sputtering) samples are shown in Figure S3. Cu mostly stays as a mixture of Cu^0,

Cu^{+} and Cu^{2+} in the as-spun sample. As expected, its contribution markedly reduces in the dealloyed ribbon. After Ar ions sputtering, clear Cu peaks emerge again, in agreement with the results from Table 1; i.e., Cu is not fully removed but a moderate amount (20 at%) remains in the material. Analysis of the core-level O 1s spectra (Figure 6b and d) is in agreement with the previously observed features. Fe and Cu oxides are present both at the surface of the as-spun (Figure S2b) and dealloyed (Figure 6b) ribbons with some differences. Namely, the relative fraction of Cu oxides is higher in the as-spun sample, in accordance to the favored removal of Cu during dealloying. After sputtering the dealloyed ribbon with Ar ions, the O signal clearly decreases (Figure 6d), which is in agreement with the detection of a large proportion of Fe and Cu in the metallic state (see Figure 6c and Figure S3).

The results gleaned from XPS analyses of the ribbons can be summarized as follows: after dealloying, the surface is mainly covered by iron oxide precipitates since the Cu-rich phase is removed by selective dissolution; underneath, the amount of oxides is lowered and metallic Fe clearly emerges (in agreement with the bcc-Fe phase observed by XRD).

2.4 Fenton Reaction

In Fenton-like heterogeneous reactions, catalysis originates from the surface of the catalyst.[36] Hence, the adsorption of H_2O_2 and other reactants at the catalyst surface plays an important role. In the presence of H_2O_2, Fe^0 oxidizes to Fe^{2+} by the transfer of two electrons, as shown in Equation (1):

$$Fe^0 + H_2O_2 + 2H^+ \rightarrow Fe^{2+} + 2H_2O \quad (1)$$

In the classical Fenton reaction, the production cycle of hydroxyl radicals can be represented as follows:[37]

$$Fe^{2+} + H_2O_2 \rightarrow Fe^{3+} + OH\cdot + OH^- \quad (2)$$

$$Fe^{3+} + H_2O_2 \rightarrow Fe^{2+} + OOH\cdot + H^+ \quad (3)$$

Furthermore, the ferric ions can be reduced to ferrous ions by the ZVI surface, hence promoting the sustained production cycle of hydroxyl radicals:

$$2Fe^{3+} + Fe^0 \rightarrow 3Fe^{2+} \quad (4)$$

In this work, both as-spun and dealloyed nanoporous Fe-rich ribbons show iron oxides and ZVI (the latter in a smaller amount) on the surface. The sustainability of the hydroxyl generation cycle [Equation (1) ~ (3)] thus depends on the ease of ferrous ion availability. In this sense, acidity is a crucial parameter for the Fenton oxidation. OH· radicals cleave azo bonds (–N=N–) in MO previously adsorbed on the catalyst surface, leading to decolorization of the dye solution (Figure 1). The sorption rate can be one of the main controlling factors during the whole catalytic oxidation reaction.[37]

2.4.1 Catalytic Performance of the Ribbons

The catalytic performance of the ribbons was investigated by following the decomposition of MO in an aqueous solution at pH 3 and at [MO]:[H_2O_2]:[Fe^{2+}] given by:[38]

[MO]:[H_2O_2]:[Fe^{2+}]

1 : 2 : 0.29

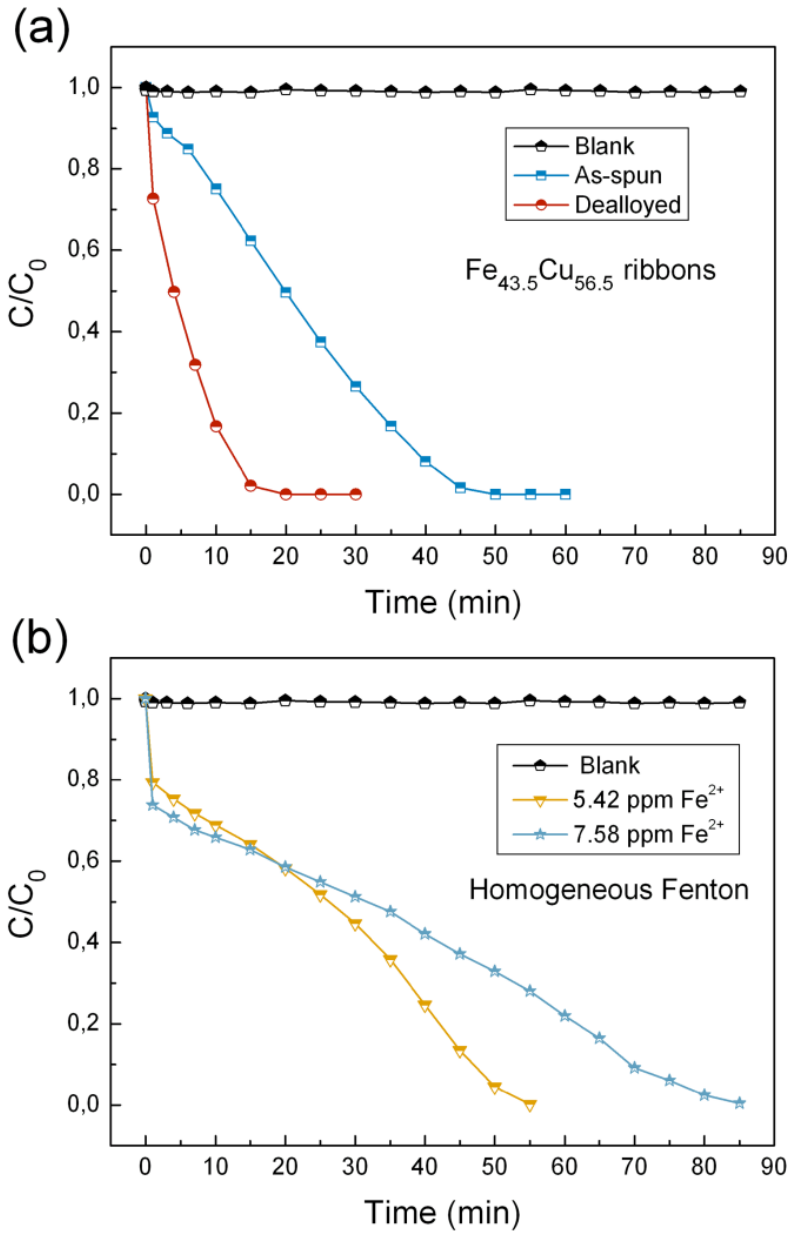

Figure 7. Dependence of the MO concentration as a function of time (i.e., removal efficiency of MO) for (a) the as-spun and dealloyed ribbons and (b) salt solutions (homogeneous Fenton) with the same concentration of Fe ions as the ones obtained after long-term immersion of the heterogeneous catalysts. All experiments were performed at room temperature for 1 h, at pH 3 and adding 0.1 g L^{-1} H_2O_2, 50 mg L^{-1} MO.

Figure 7a shows the removal efficiency of MO in aqueous solution for both as-spun and dealloyed ribbons, as well as the behavior of a blank solution without catalyst. The results reveal that the dealloyed nanoporous ribbon is much more efficient than the as-spun ribbon in degrading MO. Full degradation of MO occurs in less than 20 min when using the dealloyed ribbon, while it takes about 50 min to completely degrade the dye in presence of the as-spun ribbon. As expected, no significant degradation of MO was observed in the absence of catalyst, which was taken as a reference (blank).

Additionally, ICP measurements obtained from the aqueous solution after Fenton reaction reveal that dissolution of iron from the ribbons occurs during the experiments (see Table 3). Actually, the Fe dissolution is higher in the porous dealloyed sample, since 7.58 ppm of Fe are found in this case, while only 5.42 ppm of Fe are detected for the as-spun sample after Fenton, which could be explained by the increase of surface area-to-volume ratio in the nanoporous dealloyed ribbons. The production of ferrous ions accelerates the decomposition of H_2O_2 and the degradation of MO as the Fenton process proceeds, suggesting a combination of heterogeneous and homogeneous degradation reactions when the Fe-based alloys are used.[39] In order to assess the contribution of dissolved iron to the overall degradation process of MO, additional Fenton reactions were performed using $FeSO_4$ as the iron source. Salt dosages were calculated to provide 7.58 and 5.42 ppm Fe concentrations. As shown in Figure 7b, a rapid degradation of MO within the first minute of the assay is observed at both iron concentrations. After this point, reaction rates slow down significantly until the complete degradation of MO. This effect might be explained by the Fe^{3+}/Fe^{2+} cycle. Thus, when ferrous iron is used, the initial rate of H_2O_2 decomposition is very rapid as well as that of $OH\cdot$ and Fe^{3+} production (Equation (2)). However, with the rapid exhaustion of Fe^{2+}, the rate of $OH\cdot$ production also decreases. At this stage, the

concentration of ferrous ions depends on the decomposition reaction of Fe^{3+} in presence of H_2O_2 (Equation (3)) and this reaction is much slower than the former one.

Material	Fe, ppm	Cu, ppm
Polished as-spun ribbon	5.42	0.73
Dealloyed ribbon	7.58	1.78

Table 3 Dissolved Fe and Cu amounts during the Fenton reaction measured by ICP.

As expected, the experiment at the highest iron concentration gives the fastest degradation rate. However, when comparing the results of the two sets of experiments ($FeSO_4$ and Fe-based ribbons) it was observed that the overall process for complete elimination of MO takes longer for $FeSO_4$ than for their corresponding Fe-based ribbons counterparts. This result indicates that the use of Fe-based alloys is advantageous compared to the use of conventional $FeSO_4$ reagent. Remarkably, an induction time might be expected in order to generate surface active iron species.[40] However, in our investigation, we did not observe any induction time for the dealloyed sample, while a short induction time could be perceived with as-spun sample (see Figure 7). In the case of the dealloyed ribbons, this means that iron species are already available from the very beginning and, thus, Fenton reaction takes place immediately.[37] The presence of iron ion species on the surface of the catalyst was actually confirmed by XPS (see Figures 6 and S2).

The enhancement of the catalytic activity of Fe-based alloys might be ascribed to its ability to generate surface hydroxyl radicals and the promotion of Fe^{2+} regeneration at the Fe-based alloy surface (Equation (4)).[41] Additionally their capacity to continuously release ferrous ions to the solution avoids the rapid consumption of Fe^{2+} and the overload of ferric ions that decreases

degradation rate in conventional Fenton processes.[42] Actually, in some heterogeneous systems where the catalytic solid materials serve as a source of metal ions, even sub-μM concentrations of dissolved metal ions contribute to increase the degradation rate of the organic contaminant.[43,44] The multiple and complex mechanisms responsible for heterogeneous Fenton reactions have not been fully elucidated yet and remain the topic of extensive investigations.[43] Finally, the higher catalytic activity of dealloyed ribbons compared to that of as-spun ones could be assigned to a combination of higher active surface and iron content. It is believed that the homogeneous Fenton mechanism induced by surface-leached iron and the heterogenous catalysis mechanism compete differently in the as-cast and porous ribbons.

2.4.2 Structural and Morphological Characterization of the Ribbons after Fenton Reaction

The XRD patterns of the as-spun and dealloyed ribbons after Fenton reaction are rather similar to each other, as shown in Figure 8. The main peaks can be assigned to *fcc*-Cu, Cu_2O and η-Fe_2O_3 (JCPDS Card No. 21-0920) phases. It is thus clear that bcc-Fe tends to dissolve into the solution during the Fenton process, in agreement with ICP analyses (section 3.4.1). The relative intensity of η-Fe_2O_3 peaks is a bit higher for the as-spun ribbons, suggesting that dissolution of Fe is more pronounced in the dealloyed ribbon, probably because of its inherent nanoporosity (also in agreement with ICP analyses). The surfaces of as-spun and dealloyed ribbons after Fenton reaction are covered by Cu oxides, as confirmed by EDX (Table 1).

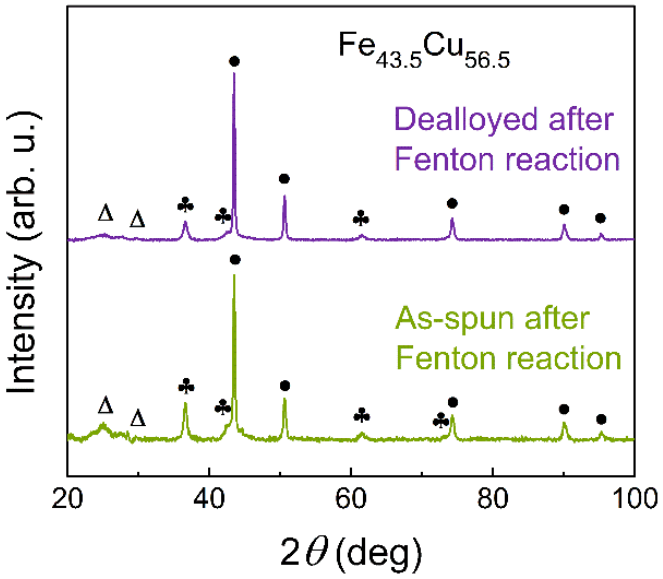

Figure 8. XRD patterns of as-spun and dealloyed ribbons after Fenton reaction. The peaks correspond to *fcc*-Cu (•), Cu_2O (♣) and η-Fe_2O_3 (Δ) phases separately.

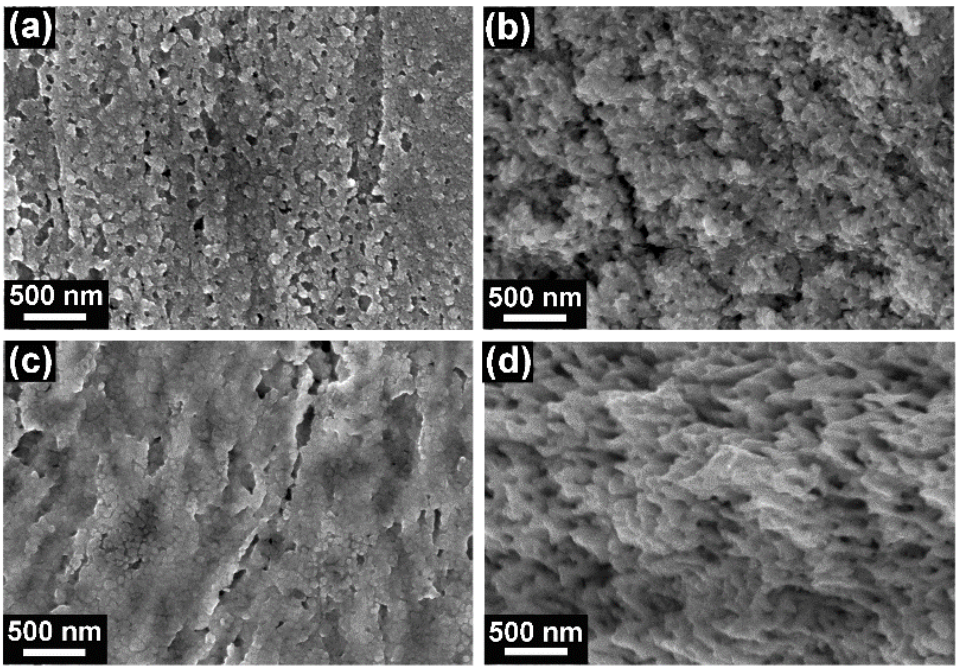

Figure 9. SEM images taken after Fenton reaction on: (a) wheel-side and (b) fracture cross-section of the as-spun ribbon; (c) wheel-side and (d) cross-section of the dealloyed ribbon.

In addition, the surface morphology after Fenton reaction becomes denser than that before Fenton (cf. Figure 9 and c), particularly in the dealloyed ribbon. The cross section images (Figure 9b and d) show that, inside the ribbons, morphology remains similar to that before Fenton reaction, i.e., the dealloyed ribbons exhibit a more obvious nanoporosity. Furthermore, according to EDX, the signal from Fe is very weak after Fenton. A rather low amount of Fe could be detected (2 ~ 3 at% for as-spun and dealloyed ribbons after Fenton reaction, respectively). Remarkably, in spite of the partial dissolution of the dealloyed ribbons during Fenton reaction, their mechanical integrity was preserved, so that the ribbons could be in any case manipulated, even after Fenton studies, for further detailed structural and magnetic characterization. The magnetic hysteresis loops of the samples after Fenton reaction are displayed in Figure S4 and the corresponding relevant parameters are listed in Table 2. Compared to the samples before Fenton, it is obvious that the saturation magnetization of the ribbons after Fenton reaction decreases significantly. However, clear hysteresis loops with well-defined values of M_r and H_c (inset of Figure S4) indicate there is an obvious ferromagnetic/ferrimagnetic contribution, which probably stems from the η-Fe_2O_3 phase detected by XRD.[45] The lower M_s of the dealloyed ribbon after Fenton sample is probably the consequence of the smaller percentage of η-Fe_2O_3 phase in this sample as compared to the as-spun ribbon after Fenton, as discussed above.

2.4.3 Surface Analysis of the Ribbons after Fenton Reaction

From the general XPS surface spectra acquired after Fenton reaction (Figure 5), the intensity of the Fe peaks is found to significantly decrease for both as-spun and dealloyed ribbons. This result is even more obvious on analyzing the high resolution Fe 2p region (see Figure S5a and Figure 10a). The deconvoluted contributions indicate the presence of oxidized iron in both cases.

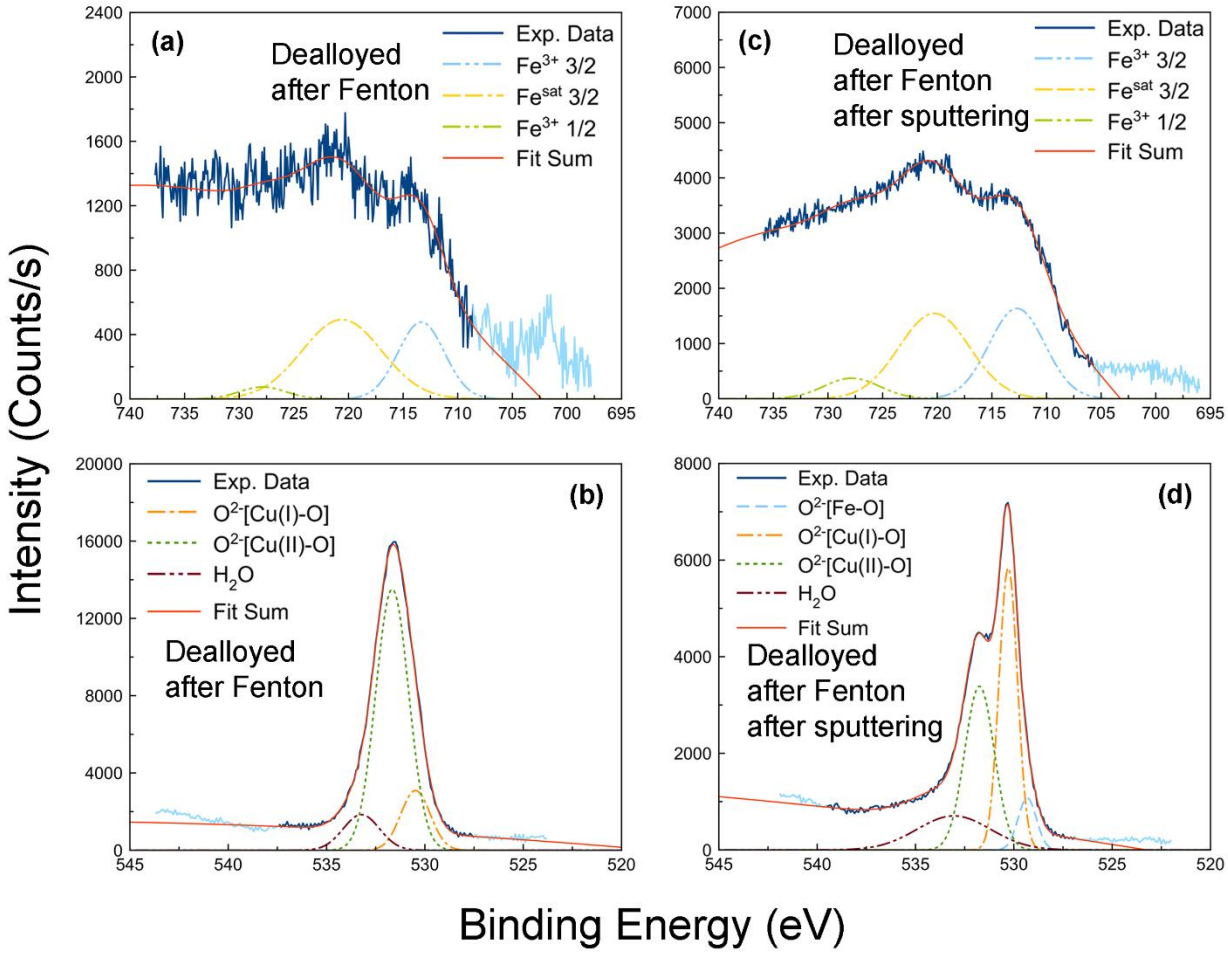

Figure 10. Experimental and deconvoluted high resolution XPS spectra of (a) Fe 2p and (b) O 1s at surface level, and of (c) Fe 2p and (d) O 1s after 1 min Ar ions sputtering for the dealloyed ribbon after Fenton reaction.

After Ar ions sputtering, the Fe signal increases but it still remains low. This is in agreement with the remarkable leaching of Fe ions during Fenton reaction. The core-level Cu 2p (Figure S6) and O 1s (Figure S5b, d and Figure 10b, d) spectra of the two ribbons after Fenton reaction are very similar, either at the uttermost surface or deeper inside the material (i.e., after Ar ions sputtering). Accordingly, the resulting surfaces after Fenton reaction are mostly composed of Cu

oxides. Interestingly, the Cu(II)/Cu(I) ratio is larger at the surface, indicating that the oxidation degree is higher, as expected from the Fenton reaction.

3. Conclusions

Fully nanoporous Fe-rich ribbons, with bcc crystallographic structure and pore size ranging between 50 and 500 nm, have been obtained by selective dissolution of the *fcc*-Cu phase from phase-separated $Fe_{43.5}Cu_{56.5}$ ribbons previously prepared by melt spinning. The nanoporous Fe-rich alloy possesses higher M_s and slightly higher M_r and H_c than the ribbons before dealloying, which can be ascribed to the removal of the paramagnetic Cu-rich phase. The ferromagnetic properties of these ribbons might be used to magnetically guide them toward specific locations in polluted water tanks in order to degrade organic matter. The dealloyed ribbons exhibited sufficient mechanical integrity during the Fenton's reaction processes, so that magnetic guiding could indeed be accomplished. Remarkably, the nanoporous dealloyed material is found to be very efficient in degrading MO in an aqueous solution at pH 3, thus acting as an efficient heterogeneous Fenton catalyst. The time needed to fully degrade MO when using the dealloyed ribbon is reduced by roughly a factor 2 as compared to the as-spun FeCu ribbons. The efficiency of this catalyst also surpasses that of homogeneous Fenton reaction when using analogous Fe cations concentrations in the aqueous media. The higher catalytic activity of dealloyed ribbons is likely due to its higher surface area and the high iron content. Overall, their ability to generate surface hydroxyl radicals, the regeneration of Fe^{2+} at their surface, and the sustained release of ferrous ions into the solution avoid the rapid consumption of Fe^{2+} and the overload of ferric ions responsible for the decreased degradation rate in conventional Fenton processes. The combination of highly efficient catalytic activity together with the convenient production

processing makes this nanoporous Fe-rich alloy an interesting candidate material for Fenton catalysis.

4. Experimental Procedure

4.1 Synthesis

Alloy ingots with nominal composition $Fe_{43.5}Cu_{56.5}$ were prepared by arc-melting mixtures of the high-purity Fe (99.95 wt%), Cu (99.95 wt%) metals in a Ti-gettered argon atmosphere (the exact alloy composition was determined by EDX, as shown in table 1). Then, a few pieces of the ingots were remelted and injected into a Cu single-roller. About 1.5 mm wide and 20 ~ 25 μm thick ribbons were produced by melt-spinning in an argon atmosphere. Subsequently, the ribbons were cut into pieces of 30 ~ 40 mm in length, which were mechanically polished using 4000 grit SiC paper and ultrasonically cleaned in distilled water for 3 min before dealloying. Selective dissolution to obtain the nanoporous ribbon was performed by electrochemical treatment in 0.065 M HNO_3 solution with an applied voltage of 14 V for 5 min, followed by washing in distilled water (see Figure 1). Both the electrolyte composition and the applied voltage were selected based on the electrochemical behavior of the individual elements according to the standard Pourbaix diagrams.[29,46]

4.2 Characterization

Structural characterization of as-spun and dealloyed samples was carried out by XRD on a Philips X'Pert diffractometer with a pixel 1D detector in the 20-100° 2θ range (step size = 0.026°, total time = 2000 s) using Cu Kα radiation (λ = 0.154178 nm). The surface morphology and fracture cross-section of the ribbons was observed by FESEM (Zeiss Merlin). Hysteresis

loops were recorded at room temperature by means of a vibrating sample magnetometer (VSM) from MicroSense. XPS experiments were performed in a PHI 5500 Multitechnique System (from Physical Electronics) with a monochromatic X-ray source (KαAl line of 1486.6 eV energy and 350 W) under ultra-high vacuum (UHV), with pressure between $5x10^{-9}$ and $2x10^{-8}$ Torr, placed perpendicular to the analyser axis and calibrated using the $3d^{5/2}$ line of Ag with a full width at half maximum (FWHM) of 0.8 eV. The analyzed area was a circle of 0.8 mm diameter for each sample. The selected resolution for the spectra was 187.85 eV of pass energy and 0.8 eV/step for the general spectra, and 23.5 eV of pass energy and 0.1 eV/step for the detailed spectra of the different elements. Composition depth profiles of the dealloyed sample were obtained by sputtering the surface with Ar+ ions (4 keV energy) for 1 minute (about 5 ~ 10 nm deep from the sample's surface). Charging effects were corrected by referencing the binding energies to that of the adventitious C ls line at 284.5 eV. A linear background was assumed.[47] The energy of the deconvoluted peaks was compared with the NIST XPS database.[48]

4.3 Fenton Process and Analysis of Samples after Fenton Reaction

To evaluate the catalytic activity of the iron-based ribbon pieces, MO was used as a model dye. MO is a toxic azo dye usually found in textile wastewater that causes severe ecological impact. All chemicals for the Fenton reaction, (i.e., MO, hydrogen peroxide, sodium sulfate and sulphuric acid) were supplied by Scharlau and used without further purification. To compare the catalytic efficiency of the ribbons before and after dealloying, MO solutions with initial concentration of 50 mg L^{-1} were prepared by diluting 1g L^{-1} stock solutions in deionized water. To carry out the experiments, 1.51 mg of as-spun ribbon and 1.42 mg of dealloyed ribbon were introduced, separately, into a 100 mL MO solution. Then, 710 mg of Na_2SO_4 (final concentration 50 mM) were added to simulate natural wastewater pollutants and pH was adjusted to 3 using

H_2SO_4 (since the reported optimum pH is between 2 ~ 3 for the Fenton reaction catalyzed by ZVI).[49,50] Separately, a 0.1 g L^{-1} H_2O_2 solution was also prepared. The reaction was started by adding this H_2O_2. Mixed solutions were continuously stirred and the reaction was performed at room temperature for one hour or until complete degradation of MO was achieved. Aliquots were withdrawn every 5 or 10 minutes from the reaction beaker and the concentration of MO was measured using a Jasco V-570 UV spectrophotometer at a wavelength of 505 nm, which corresponded to the maximum absorption of the solution at the beginning of the experiment (pH 3). After that, the aliquot was placed back to the beaker. Additionally, a blank experiment was performed where no ribbon catalyst was added.

The structure, morphology and magnetic properties of the ribbons after Fenton reaction were investigated by XRD, FESEM-EDX and VSM. The concentrations of metallic cations leached into the solution after the Fenton experiments were measured by inductively coupled plasma (ICP) spectroscopy (ICPE 9000, Shimadzu). For this purpose, 17 mL and 13 mL were extracted from the reaction vessels containing as-spun and dealloyed ribbons, respectively. XPS experiments, including compositional depth measurements were performed using the same equipment, parameters and analysis methodology as mentioned above. To carry out comparative homogeneous Fenton reactions, the same procedure was applied using $FeSO_4 \cdot 7\ H_2O$ instead of Fe-based ribbons. Salt dosages were chosen to coincide with those measured by ICP at the end of the previous experiments.

Associated Content

Supporting Information. Additional details and figures as mentioned in the text. This material is available free of charge.

Author Information

Corresponding Authors

Email: *eva.pellicer@uab.cat; §jordi.sort@uab.cat

Author Contributions

The manuscript was written through contributions from all authors: Huiyan Zhang, Eva Pellicer and Jordi Sort conceived and designed this work. Huiyan Zhang and Yuping Feng executed the dealloying process and characterization measurements. The original ribbon samples were prepared and provided by Yangyang Cheng and Tao Zhang. Ainhoa Altube, Eva García-Lecina and Francisco Alcaide performed the Fenton reaction. Huiyan Zhang wrote the draft. Eva Pellicer, Jordi Sort, Maria Dolors Baró, Eva García-Lecina and Francisco Alcaide reviewed and edited the draft. All authors have given approval to the final version of the manuscript.

Acknowledgements

This work has been partially funded by the the Generalitat de Catalunya (2014-SGR-1015) and the Spanish Ministerio de Economía y Competitividad (MAT2014-57960-C3-1-R, co-financed by the Fondo Europeo de Desarrollo Regional, FEDER; and MAT2014-57960-C3-2-R). Yuping Feng is grateful for his CSC Grant. Dr. Eva Pellicer is grateful to MINECO for the "Ramon y Cajal" contract (RYC-2012-10839).

References

(1) Ikehata, K.; El-din, M. G. M. Aqueous Pesticide Degradation by Hydrogen Peroxide/Ultraviolet Irradiation and Fenton-Type Advanced Oxidation Processes: A Review. *J. Environ. Eng. Sci.* **2006**, *5*, 81-135.

(2) Georgi, A.; Kopinke, F. D. Interaction of Adsorption and Catalytic Reactions in Water Decontamination Processes: Part I. Oxidation of Organic Contaminants with Hydrogen Peroxide Catalyzed by Activated Carbon. *Appl. Catal. B Environ.* **2005**, *58*, 9-18.

(3) Yoshida, Y.; Ogata, S.; Nakamatsu, S.; Shimamune, T.; Kikawa, K.; Inoue, H.; Iwakura, C. Decoloration of Azo Dye Using Atomic Hydrogen Permeating Through a Pt-Modified Palladized Pd Sheet Electrode. *Electrochim. Acta* **1999**, *45*, 409-414.

(4) Dutta, K.; Mukhopadhyay, S.; Bhattacharjee, S.; Chaudhuri, B. Chemical Oxidation of Methylene Blue Using a Fenton-Like Reaction. *J. Hazard. Mater.* **2001**, *84*, 57-71.

(5) Gogate, P. R.; Pandit, A. B. A Review of Imperative Technologies for Wastewater Treatment I: Oxidation Technologies at Ambient Conditions. *Adv. Environ. Res.* **2004**, *8*, 501-551.

(6) Casero, I.; Sicilia, D.; Rubio, S.; Perez-Bendito, D. Chemical Degradation of Aromatic Amines by Fenton's Reagent, *Water Res.* **1997**, *31*, 1985-1995.

(7) Kuo, W. G. Decolorizing Dye Wastewater with Fenton's Reagent. *Water Res.* **1992**, *26*, 881-886.

(8) Nam, S.; Renganathan, V.; Tratnyek, P. G. Substituent Effects on Azo Dye Oxidation by the Feiii–EDTA–H_2O_2 System. *Chemosphere* **2001**, *45*, 59-65.

(9) Barbusiński, K. The Modified Fenton Process for Decolorizationof Dye Wastewater *Polish J. Environ. Stud.* **2005**, *14*, 281-285.

(10) Huston, P. L.; Pignatello, J. J. Degradation of Selected Pesticide Active Ingredients and Commercial Formulations in Water by the Photo-Assisted Fenton Reaction. *Water Res.* **1999**, *33*, 1238-1246.

(11) Lin, S. H.; Lin, C. M.; Leu, H. G. Operating Characteristics and Kinetic Studies of Surfactant Wastewater Treatment by Fenton Oxidation. *Water Res.* **1999**, *33*, 1735-1741.

(12) Liou, M. J.; Lu, M. C.; Chen, J. N. Oxidation of Explosives by Fenton and Photo-Fenton Processes. *Water Res.* **2003**, *37*, 3172-3179.

(13) Brillas, E.; Sirés, I.; Oturan, M. A. Electro-Fenton Process and Related Electrochemical Technologies Based on Fenton's Reaction Chemistry. *Chem. Rev.* **2009**, *109*, 6570-6631.

(14) Arnold, S. M.; Hickey, W. J.; Harris, R. F. Degradation of Atrazine by Fenton's Reagent: Condition Optimization and Product Quantification. *Environ. Sci. Technol.* **1995**, *29*, 2083-2089.

(15) Zazo, J. A.; Casas, J. A.; Mohedano, A. F.; Rodríguez, J. J. Catalytic Wet Peroxide Oxidation of Phenol with a Fe/Active Carbon Catalyst. *Appl. Catal. B Environ.* **2006**, *65*, 261-268.

(16) Sharma, V. K. Ferrate (VI) and Ferrate (V) Oxidation of Organic Compounds: Kinetics and Mechanism. *Coord. Chem. Rev.* **2013**, *257*, 495-510.

(17) Hartmann, M.; Kullmann, S.; Keller, H. Wastewater Treatment with Heterogeneous Fenton-Type Catalysts Based on Porous Materials. *J. Mater. Chem.* **2010**, *20*, 9002-9017.

(18) Xu, H. Y.; Qi, S. Y.; Li, Y.; Zhao, Y.; Li, J. W. Heterogeneous Fenton-Like Discoloration of Rhodamine B Using Natural Schorl as Catalyst: Optimization by Response Surface Methodology. *Environ. Sci. Pollut. Res.* **2013**, *20*, 5764-5772.

(19) Karthikeyan, S.; Titus, A.; Gnanamani, A.; Mandal, A. B.; Sekaran, G. Treatment of Textile Wastewater by Homogeneous and Heterogeneous Fenton Oxidation Processes. *Desalination* **2011**, *281*, 438-445.

(20) Fontecha-Cámara, M. A.; Álvarez-Merino, M. A.; Carrasco-Marín, F.; López-Ramón, M. V.; Moreno-Castilla, C. Heterogeneous and Homogeneous Fenton Processes Using Activated Carbon for the Removal of the Herbicide Amitrole from Water. *Appl. Catal. B Environ.* **2011**, *101*, 425-430.

(21) Calleja, G.; Melero, J. A.; Martínez, F.; Molina, R. Activity and Resistance of Iron-Containing Amorphous, Zeolitic and Mesostructured Materials for Wet Peroxide Oxidation Of Phenol. *Water Res.* **2005**, *39*, 1741-1750.

(22) Rusevova, K.; Kopinke, F. D.; Georgi, A. Nano-Sized Magnetic Iron Oxides as Catalysts for Heterogeneous Fenton-Like Reactions—Influence of Fe (II)/Fe (III) Ratio on Catalytic Performance. *J. Hazard. Mater.* **2012**, *241-242*, 433-440.

(23) Babuponnusami, A.; Muthukumar, K. Removal of Phenol by Heterogenous Photo Electro Fenton-Like Process Using Nano-Zero Valent Iron. *Sep. Purif. Technol.* **2012**, *98*, 130-135.

(24) Wang, Y.; Zhao, H.; Zhao, G. Iron-Copper Bimetallic Nanoparticles Embedded within Ordered Mesoporous Carbon as Effective and Stable Heterogeneous Fenton Catalyst for the Degradation of Organic Contaminants. *Appl. Catal. B Environ.* **2015**, *164*, 396-406.

(25) Luo, L.; Dai, C.; Zhang, A.; Wang, J.; Liu, M.; Song, C.; Guo, X. A Facile Strategy for Enhancing FeCu Bimetallic Promotion for Catalytic Phenol Oxidation. *Catal. Sci. Technol.* **2015**, *5*, 3159-3165.

(26) Wang, J.; Liu, C.; Tong, L.; Li, J.; Luo, R.; Qi, J.; Li, Y.; Wang, L. Iron–Copper Bimetallic Nanoparticles Supported on Hollow Mesoporous Silica Spheres: An Effective Heterogeneous Fenton Catalyst for Orange II Degradation. *RSC Adv.* **2015**, *5*, 69593-69605.

(27) Parmar, J.; Vilela, D.; Pellicer, E.; Esqué-de los Ojos, D.; Sort, J.; Sánchez, S. Reusable and Long‐Lasting Active Microcleaners for Heterogeneous Water Remediation. *Adv. Funct. Mater.* **2016**, *26*, 4152-4161.

(28) McCue, I.; Benn, E.; Gaskey, B.; Erlebacher, J. Dealloying and Dealloyed Materials. *Annu. Rev. Mater. Sci.* **2016**, *46*, 263-286.

(29) Park, B. J.; Chen, Y. M.; Ohkubo, T. Metallic Porous Materials' Design with Phase Separation in Fe–Cu And Co–Cu Systems. *Intermetallics* **2009**, *17*, 958-961.

(30) Niyomsoan, S.; Gargarella, P.; Chomsaeng, N.; Termsuksawad, P.; Kühn, U.; Eckert, J. Phase Separation in Rapid Solidified Ag-Rich Ag-Cu-Zr Alloys. *Mater. Res.* **2015**, *18*, 120-126.

(31) Kuncser, V.; Valeanu, M.; Lifei, F.; Predoi, D.; Jianu, A.; Kappel, W.; Codescu, M.; Patroi, E.; Pasuk, I.; Bulinski, M.; Filoti, G. Micro-Structure and Magnetic Properties of Fe–Cu Nanocomposites for Anisotropic Permanent Magnets. *J. Alloys Compd.* **2005**, *395*, 1-6.

(32) Lee, D. W.; Ryan, D. H.; Altounian, Z.; Kuprin, A. Structural and Magnetic Properties of Cu/Fe Multilayers. *Phys. Rev. B* **1999**, *59*, 7001-7009.

(33) Cullity, B. D.; Graham, C. D. *Introduction to magnetic materials*, Wiley-IEEE Press: Piscataway, USA, 2009.

(34) Sato, F.; Tezuka, N.; Sakurai, T.; Miyazaki, T. Grain Diameter and Coercivity of Fe, Ni, and Co Metals. *IEEE Transl. J. Magn. Japan* **1994**, *9*, 100-106.

(35) Li, X.; Cao, J.; Zhang, W. Stoichiometry of Cr(VI) Immobilization Using Nanoscale Zerovalent Iron (Nzvi): A Study with High-Resolution X-Ray Photoelectron Spectroscopy (HR-XPS). *Ind. Eng. Chem. Res.* **2008**, *47*, 2131-2139.

(36) Wang, N.; Zheng, T.; Zhang, G.; Wang, P. A Review on Fenton-Like Processes for Organic Wastewater Treatment. *J. Environ. Chem. Eng.* **2016**, *4*, 762-787.

(37) Shahwan, T.; Sirriah, S. A.; Nairat, M.; Boyaci, E.; Eroğlu, A.E.; Scott, T. B.; Hallam, K. R. Green Synthesis of Iron Nanoparticles and Their Application as a Fenton-Like Catalyst for the Degradation of Aqueous Cationic and Anionic Dyes. *Chem. Eng. J.* **2011**, *172*, 258-266.

(38) García-Rojas, O.; Gómez-Quintero, C.; Ríos-Bolívar, M.; Romero, A.; Rodríguez, A. Study and Modeling of Methylorange Degradation with the Fenton Reaction. *Proc. 9th WSEAS Int. Conf. Comput. Intell. Man-Machine Syst. Cybern.* **2010**, 251-258.

(39) Zhou, T.; Li, Y.; Li, J.; Wong, F-S.; Lu, X. Oxidation of 4-Chlorophenol in a Heterogeneous Zero Valent Iron/H2O2 Fenton-Like System: Kinetic, Pathway and Effect Factors. *Sep. Purif. Technol.* **2008**, *62*, 551-558.

(40) H. Hassan, H.; Hameed, B. H. Decolorization of Acid Red 1 by heterogeneous Fenton-like reaction using Fe-ball clay catalyst. *IPCBEE* **2011**, *8*, 232-236.

(41) Xiang, W.; Zhang, B.; Zhou, T.; Wu, X.; Mao, J. An Insight in Magnetic Field Enhanced Zero-Valent Iron/H_2O_2 Fenton-Like Systems: Critical Role and Evolution of the Pristine Iron Oxides Layer. *Sci. Rep.* **2016**, *6*, 24094.

(42) Carra, I.; Malato, S.; Jiménez, M.; Maldonado, M. I.; Sánchez Pérez, J.A. Microcontaminant Removal by Solar Photo-Fenton at Natural Ph Run with Sequential and Continuous Iron Additions. *Chem. Eng. J.* **2014**, *235*, 132-140.

(43) He, J.; Yang, X.; Men, B.; Wang, D. Interfacial mechanisms of heterogeneous Fenton reactions catalyzed by iron-based materials: A review. *J. Env. Sci.* **2016**, *39*, 97-109.

(44) Kuan, C.-C.; Chang, S.-Y.; Schroeder. S. L. M. Fenton-Like Oxidation of 4-Chlorophenol: Homogeneous or Heterogeneous? Ind. Eng. Chem. Res. **2015**, *54*, 8122-8129.

(45) Zhong, J.; Cao, C.; Liu, H.; Ding, Y.; Yang, J. Fabrication of Hollow and Yolk–Shell Structured η-Fe_2O_3 Nanoparticles with Versatile Configurations. *Ind. Eng. Chem. Res.* **2013**, *52*, 1303-1308.

(46) Parsons, R. Atlas of Electrochemical Equilibria in Aqueous Solutions. *J. Electroanal. Chem. Interfacial Electrochem.* **1967**, *13*, 471.

(47) Repoux, M. Comparison of Background Removal Methods for XPS. *Surf. Interface Anal.* **1992**, *18*, 567-570.

(48) NIST X-ray Photoelectron Spectroscopy Database, Version 4.1, **2012**, http//:srdata.nist.gov/xps/.

(49) Hsueh, C. L.; Huang, Y. H.; Wang, C. C.; Chen, C. Y. Degradation of Azo Dyes Using Low Iron Concentration of Fenton and Fenton-Like System. *Chemosphere* **2005**, *58*, 1409-1414.

(50) Devi, L. G.; Kumar, S. G.; Reddy, K. M.; Munikrishnappa, C. Photo Degradation of Methyl Orange an Azo Dye by Advanced Fenton Process Using Zero Valent Metallic Iron: Influence of Various Reaction Parameters and Its Degradation Mechanism. *J. Hazard. Mater.* **2009**, *164*, 459-467.

Table of Contents